

Supplementary Information

Unveil the underlying mechanism of record-high efficiency organic near-infrared photodetector harnessing a single-component photoactive layer

Miaosheng Wang^a, Ya-Ze Li^b, Hung-Cheng Chen^c, Che-Wei Liu^b, Yi-Sheng Chen^c, Yuan-Chih Lo^c,
Cheng-Si Tsao^{d,e}, Yu-Ching Huang^f, Shun-Wei Liu^{b,g,*}, Ken-Tsung Wong^{c,h,*}, and Bin Hu^{a,*}

^a *Department of Materials Science and Engineering, University of Tennessee, Knoxville, TN 37996, USA*

^b *Department of Electronic Engineering, Ming Chi University of Technology, New Taipei City 24301, Taiwan*

^c *Department of Chemistry, National Taiwan University, Taipei 10617, Taiwan*

^d *Department of Materials Science and Engineering, National Taiwan University, Taipei 106, Taiwan.*

^e *Institute of Nuclear Energy Research, Taoyuan 325, Taiwan*

^f *Department of Materials Engineering, Ming Chi University of Technology, New Taipei City 24301, Taiwan*

^g *Organic Electronics Research Center, Ming Chi University of Technology, New Taipei City 24301, Taiwan*

^h *Institute of Atomic and Molecular Science, Academia Sinica, Taipei 10617, Taiwan*

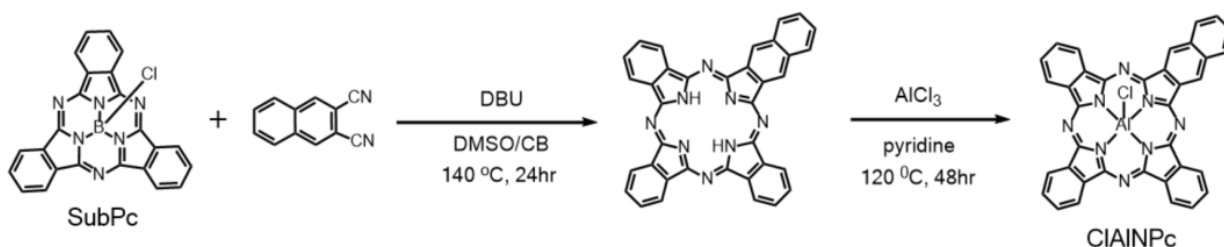
*Corresponding authors:

Shun-Wei Liu: Email: swliu@mail.mcut.edu.tw

Ken-Tsung Wong: Email: kenwong@ntu.edu.tw

Bin Hu, E-mail: bhu@utk.edu

I. Synthesis procedure of ClAlNPc :



The desired ClAlNPc compound was obtained from the metalization reaction of the unsymmetrical free-base phthalocyanine with AlCl₃. Firstly, the free-base phthalocyanine compound was prepared by the literature method.^[1] A solution of 2,3-dicyanonaphthalene (300 mg, 1.87mmol) and DBU (0.14 mL, 0.93 mmol) in dimethyl sulfoxide (DMSO)/chlorobenzene (30 mL, 5:1) was heated to 130 °C for 2h. Then, a suspension of SubPc (400 mg, 0.93 mmol) in DMSO/chlorobenzene (60 mL, 1:1) was added drop-wise to the heated mixture over a period of 1 h. Subsequently, the reaction was kept at 140 °C for 24 h. The reaction mixture was cooled to room temperature and evaporated on a rotary evaporator to remove the solvents. The water/methanol (1:1) 100 ml was poured into the concentrated reaction mixture and then the precipitated product was filtered off. The filtered compound was washed with methanol and acetone. The crude free-base phthalocyanine product and an excess (>10 equiv.) of anhydrous AlCl₃ were dissolved in the pyridine solution for the synthesis of ClAlNPc. The mixture was heated to 120 °C for 48h under a nitrogen atmosphere. After the reaction mixture was cooled to room temperature, the solvent was removed by rotary evaporation. The obtained black product was filtered and washed with acetone. The synthesized ClAlNPc product was sublimed in a temperature (350 °C) vacuum furnace to give pure compound 346 mg (59%, calculated by SubPC) as a deep-blue powder.

II. CIAIPc-based single-component active layer NIR OPDs:

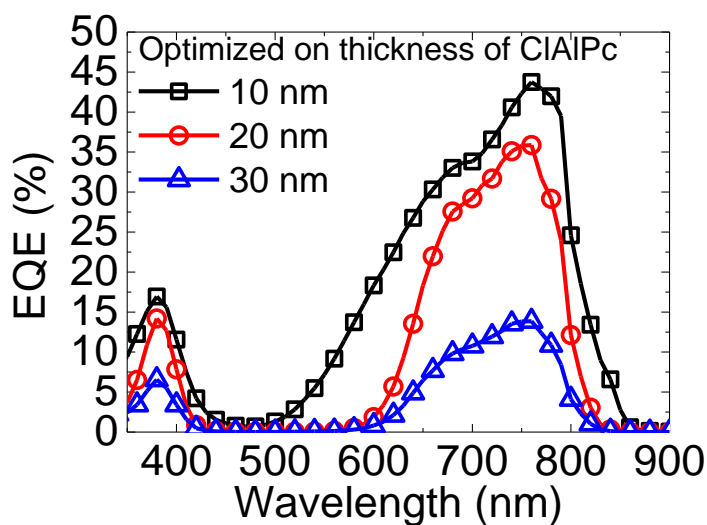


Figure S1. The EQE (under 3 V bias) of optimized single layer CIAIPc-OPD as followed structure with: ITO/ CIAIPc (X nm)/ TAPC (90 nm)/ MoO₃ (15 nm)/ Al (120 nm), where X=10, 20, 30 nm.

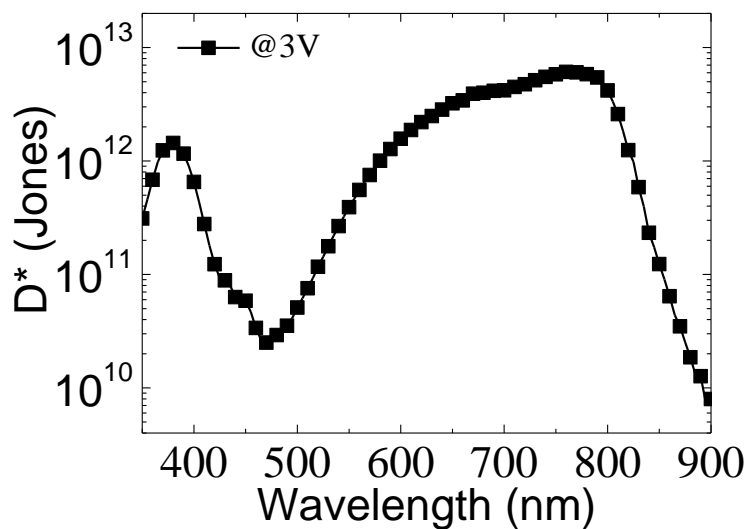


Figure S2: The specific detectivity of the CIAIPc photodetector at forward bias of 3 V.

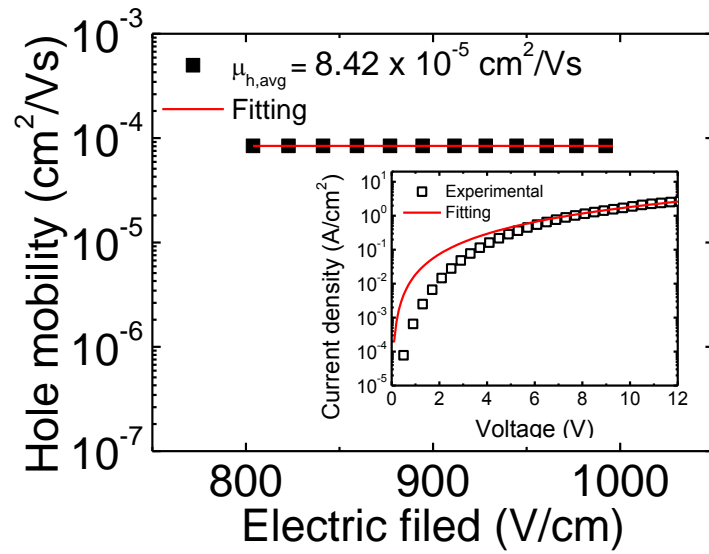


Figure S3: Mobility of ClAlPc.

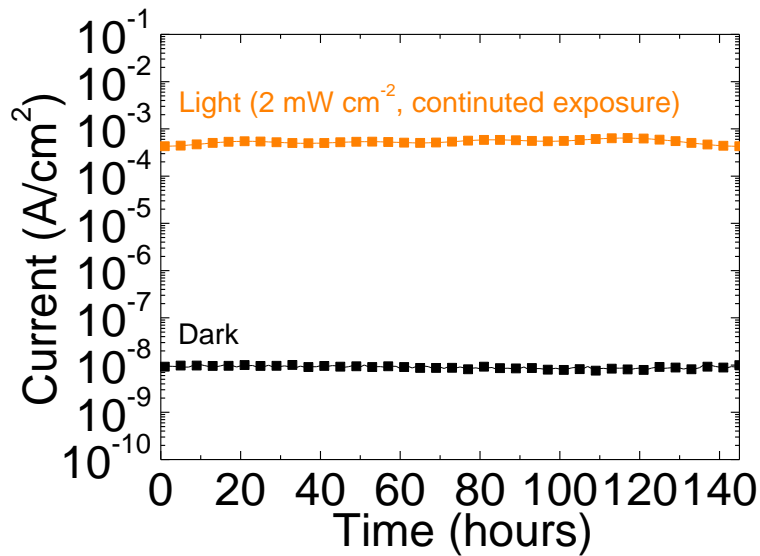


Figure S4: The aging study for stability test of ClAlPc-based OPD. Light and dark current density exposed and biased (3 V) continuously as a function of time. The data was recorded with 1 hour interval.

III. Single-component layer photovoltaic devices:

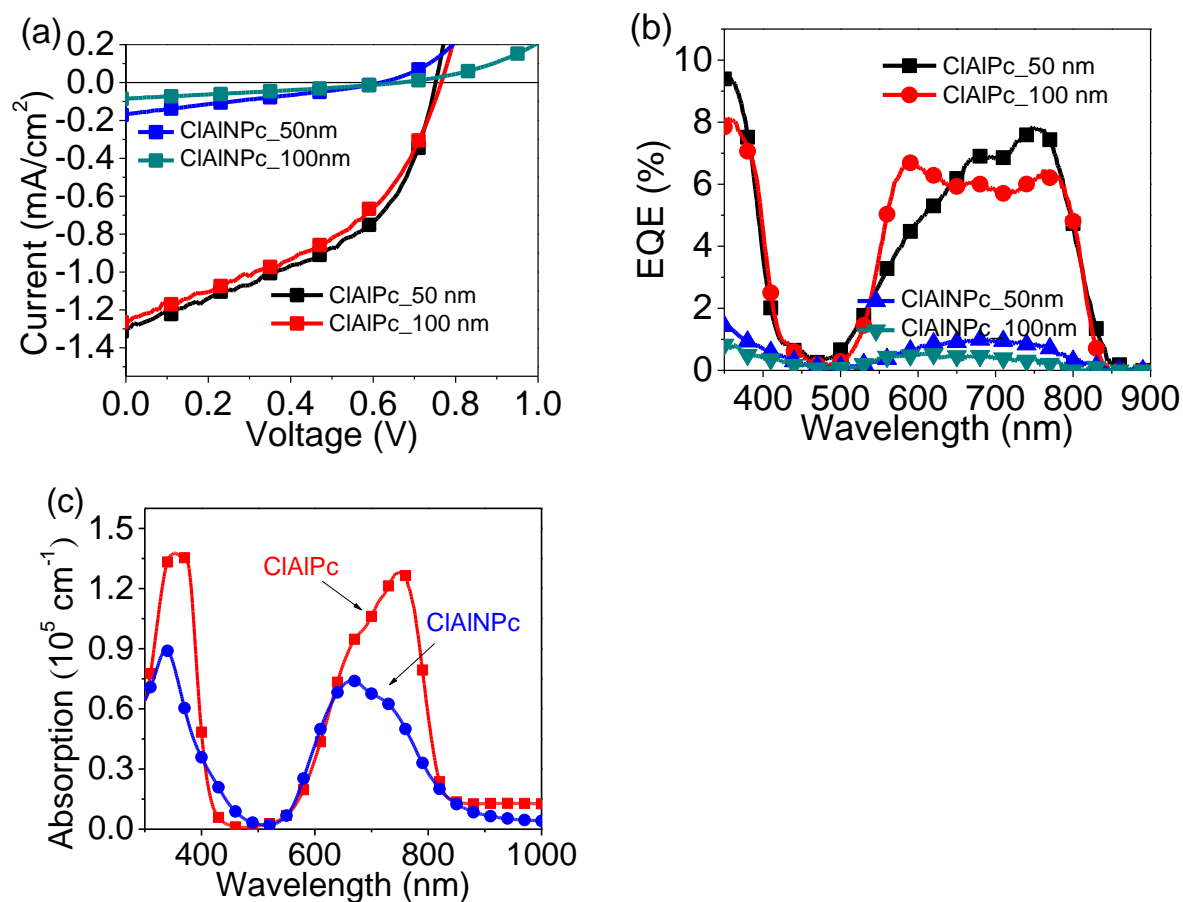


Figure S5. Device performance characterization. (a) I-V curves under one sun condition for single-layer CIAIPc and CIAINPc devices (ITO/CIAIPc/AI and ITO/CIAINPc/AI). (b) EQE for ITO/CIAIPc or CIAINPc/AI devices. (c) Absorption spectra of CIAIPc and CIAINPc thin films with the same thickness (50 nm).

Table S1: Photovoltaic parameters of CIAIPc and CIAINPc single active layer devices

Device	V_{oc} (V)	J_{sc} (mA/cm ²)	FF (%)	PCE (%)
CIAIPc 50nm	0.76	1.3	45.42	0.45
CIAIPc 100nm	0.77	1.27	42.9	0.42
CIAINPc 50nm	0.62	0.17	26.36	0.03
CIAINPc 100nm	0.67	0.09	28.59	0.02

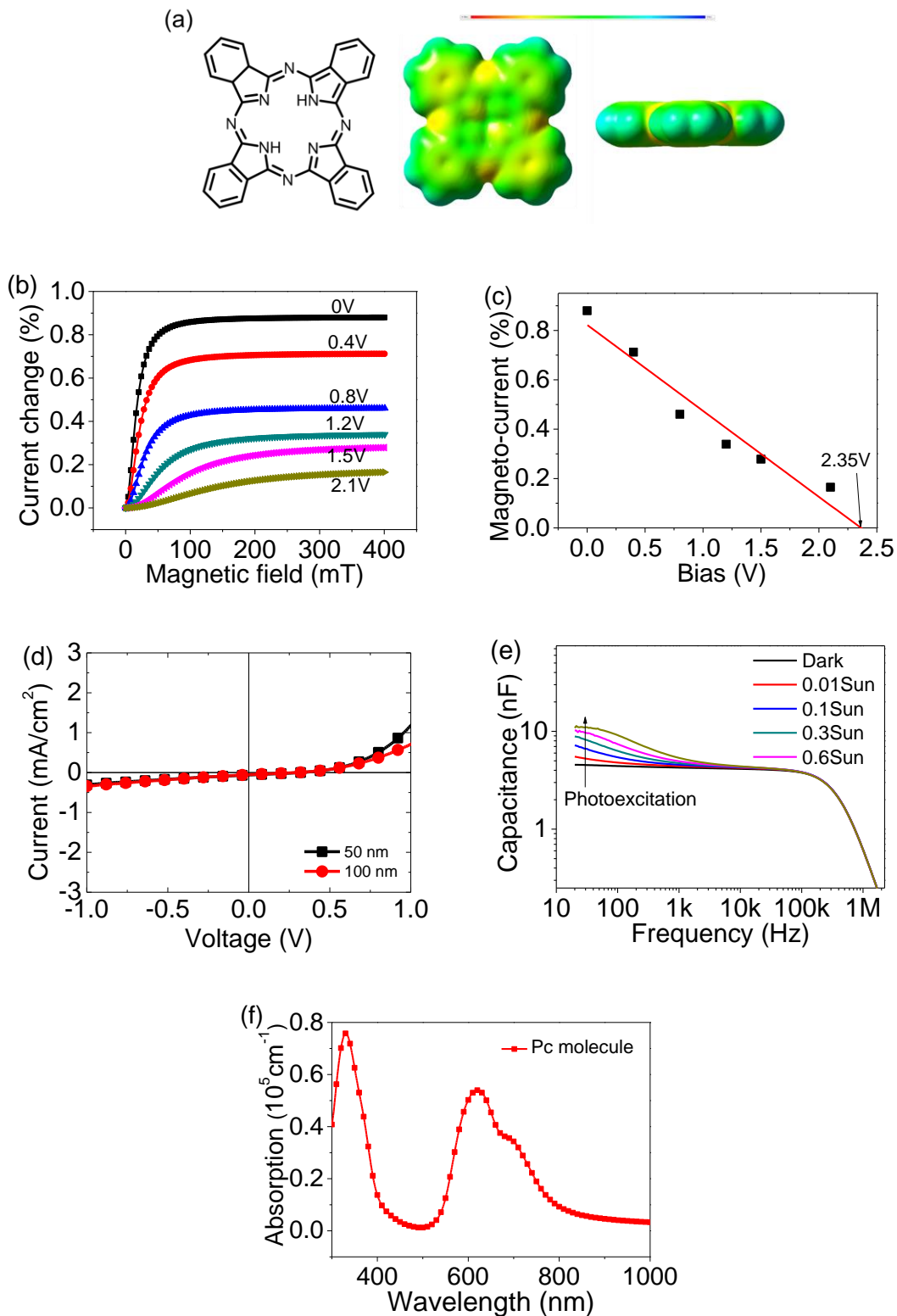


Figure S6: (a) Symmetrically arranging four isoindole rings of Pc and the calculated excited state electrostatic potential maps of CIAIPc and CIAINPc; (b) bias-dependent magneto-photocurrent

and (c) maximum magnitude of magneto-photocurrent as the function of applied reverse bias for single-layer device (ITO/Pc 50 nm/Al); (d) I-V curves under one sun condition for single-layer Pc devices (ITO/Pc 50 or 100 nm/Al); (e) C-f curves under simulated sunlight with variable intensities for single-layer device (ITO/Pc 50 nm/Al); (f) Absorption spectrum of Pc molecule thin films (50nm).

IV. X-ray characterizations on ClAlPc thin films:

Figure S7(a~c) shows the 2D grazing-incidence wide-angle X-ray scattering (GIWAXS) patterns of the ClAlPc films with the thicknesses of 10, 30 and 50 nm on ITO-coated Si substrates, respectively. Figure S7(d~f) shows the 1D GIWAXS profiles of these films corresponding to Figure S7(a~c). The GIWAXS profile of the 10-nm-thick ClAlPc film on the ITO-coated Si substrate has a main peak at $Q = 0.48 \text{ \AA}^{-1}$ from (001) plane (corresponding to $2\theta = 6.84^\circ$, d spacing = 12.9 \AA) of nanoscale film crystallites or grain which is consistent with the crystalline structure of ClAlPc reported by Wynne (CCDC No. 1134071) and X-ray diffraction analysis of bulk ClAlPc materials^[2]. The peak at $Q = 0.95 \text{ \AA}^{-1}$ is the (002) plane peak. However, The GIWAXS profiles of the 30-nm-thick and 50-nm-thick ClAlPc films demonstrate the main peak at $Q = \sim 0.41 \text{ \AA}^{-1}$ for (001) plane and the second-order peak at $Q = \sim 0.85 \text{ \AA}^{-1}$ for (002) plane. It is noted that the shift of (001) peak toward the low-Q and the d spacing largely increases with increasing film thickness from 30 to 50 nm. This effect may be closely related to the increased contact with the surrounding amorphous zone (between nanoscale ClAlPc grains) revealed by the GISAXS study (discussed later). The 2D GIWAXS patterns show the orientation of (001) plane in the nano film crystallites, indicated by the diffraction spots, has an angle of 45 degree about the substrate or film surface (on the Q_{xy} direction) for all thicknesses. The arc length of diffraction spots increases for the 30- and 50-nm-thick films, representing the slight vibration of orientation of the nanoscale ClAlPc film grains formed on the substrate surface.

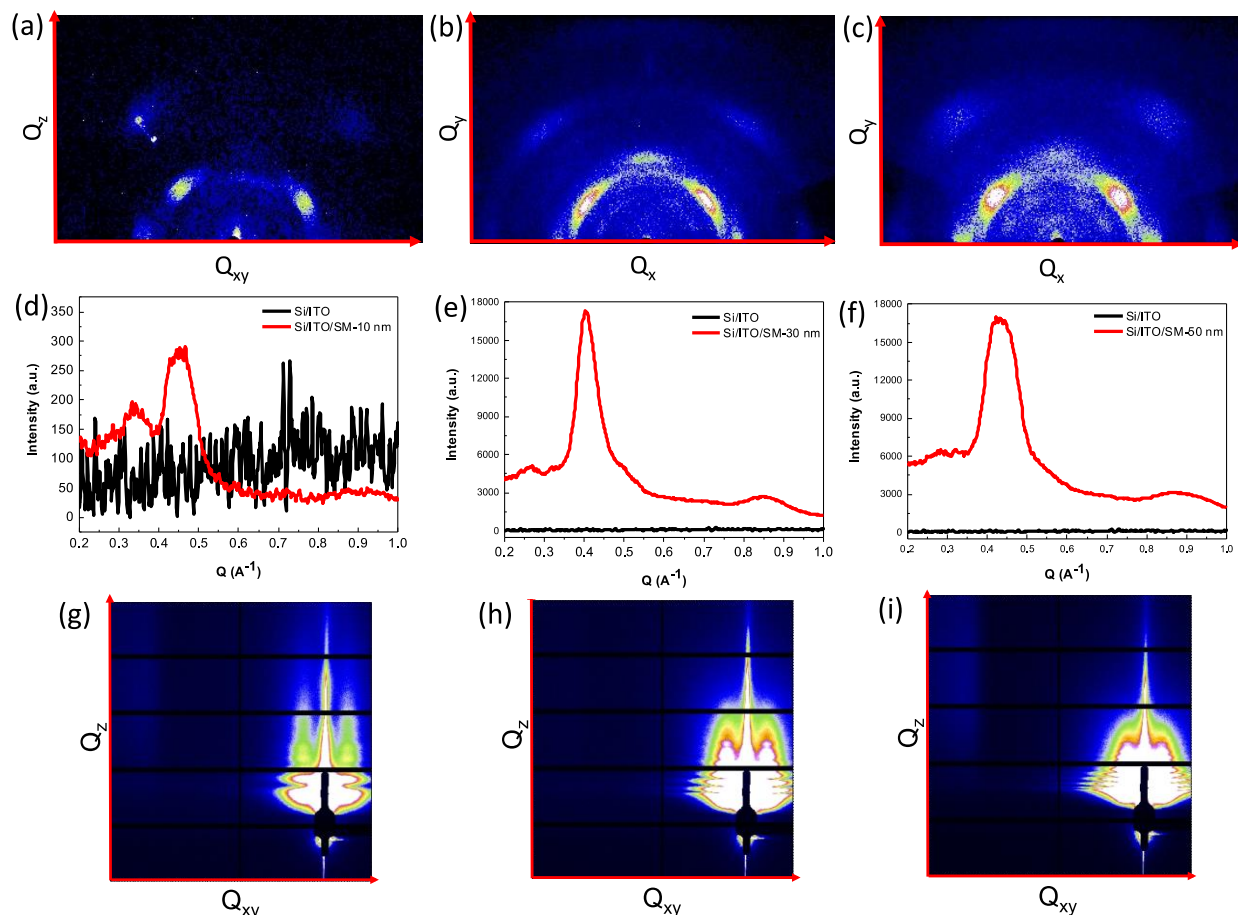


Figure S7. (a~c) 2D GIWAXS patterns of the CIAIPc films on ITO-coated Si substrate with thicknesses of 10, 30 and 50 nm, respectively. (d~f) The reduced GIWAXS profiles corresponding to (a~c). (g), (h) and (i) 2D GISAXS patterns corresponding to the film thicknesses of 10, 30 and 50 nm, respectively.

According to the previous grazing-incidence small-angle X-ray scattering (GISAXS) and GIWAXS study on the CuPc film morphology,^[3,4] the deposited CuPc films consists of the disk-shape CuPc crystal nanograins and the amorphous region between grains. As shown in the 2D GISAXS patterns of the CIAIPc films with different thickness (Figure S7 g-i), two intensity streaks (or two wings) split from the central diffraction along the Q_z direction is originated from the interference effect between CIAIPc nanograins. The average distance between the CIAIPc nanograins in the horizontal direction in the film is closely related to the peak positions of the wings along the Q_{xy} direction. The Q_z (out-of-plane) and Q_{xy} (in-plane) directions are the directions normal to and parallel to the substrate or film surface, respectively. The strong intensity of wing

peak of the 10-nm-thick ClAlPc film, as shown in Figure S7g, represents the high degree of simple periodic or equal-spacing arrangement of nanograins on the substrate. However, the wing intensity become weak with increasing film thickness up to 50 nm (Figure S7h and i), signifying the less periodically separated or more random distributed nanograins in the horizontal direction in the thicker films. Moreover, there is appearance of several increasing peaks normal to central diffraction peak along the Q_{xy} direction, signifying the formation of sub-layers parallel to film surface. Each sub-layer consists of the horizontally distributed nanograins. Apparently, the variation of 2D GISAXS patterns with film thickness directly evidences the formation, growth and spatial arrangement of ClAlPc nanograins during film deposition process.

For quantitatively determine the nanostructure in the bulk ClAlPc films, the in-plane GISAXS profiles are reduced from the Yoneda peak along the Q_{xy} direction at $Q_z = 0$ of 2D GISAXS patterns.^[5,6,7] The GISAXS profiles of the ClAlPc films on the ITO-coated Si substrate with different thicknesses, as shown in Figure S8, shows the peak contributed by structure factor. The average distance between the ClAlPc nanograins in the horizontal direction in the film can be approximately estimated by the peak position $Q_{\max} (=2\pi/Q_{\max})$.^[8,9] The average distances between nano grains for the ClAlPc films with thicknesses of 10, 30 and 50 nm are determined to be ~ 37 , 48 and 50 nm, respectively. The GISAXS profile contributed by the disk-like ClAlPc nanograins in the bulk film can be expressed by the product of hard-sphere-model structure factor^[10,11] and form factor of cylinder. The form factor of cylinder $P(Q)$ ^[8,9] with a radius, R , and thickness, T , can be given by

$$P(Q) = \Delta\rho^2(\pi R^2 T) \int_0^{\frac{\pi}{2}} \left[2j_0\left(\frac{QT}{2} \cos \alpha\right) \frac{J_1(QR \sin \alpha)}{(QR \sin \alpha)} \right]^2 \sin \alpha d\alpha \quad \dots \dots (1)$$

where $\Delta\rho$ denotes the scattering length density contrast between the cylinder and matrix. The integral over α averages the form factor over all possible orientations of the cylinder with respect to Q . $j_0(x)$ and $J_1(x)$ are zero-order spherical Bessel function and first-order Bessel function, respectively. The upturn intensity in the low- Q region of GISAXS profiles can be fitted by the power law with an exponent of ~ 3.0 , demonstrating the fractal surface of film. The fitted radius and thickness of the 10-nm-thick ClAlPc film are 13.3 and 11 nm, respectively. The fitted radius

and thickness of the 30-nm-thick ClAlPc film are 22.0 and 13 nm, respectively. The fitted radius and thickness of the 50-nm-thick ClAlPc film are 24.0 and 12 nm, respectively. Based on the analysis of 2D GISAXS patterns and GISAXS profiles, the size and orientation and distribution of the disk-like ClAlPc grains in the film with different thicknesses can be schematically illustrated in Figure S9. The region between nanograin is the amorphous ClAlPc molecules and micropores.

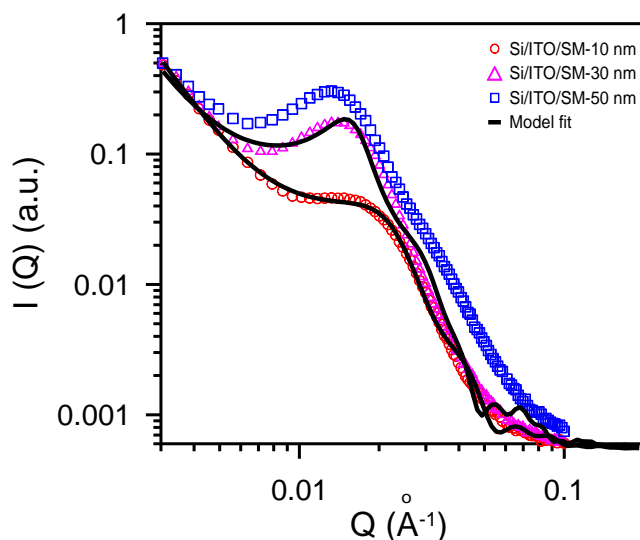


Figure S8. GISAXS profiles of the ClAlPc films on ITO-coated Si substrate with film thicknesses of 10, 30 and 50 nm in comparison with the model-fitting intensity (solid lines).

As shown in Figure S9, we propose a growth and morphological evolution model of the ClAlPc nanograin as a function of film thickness. For the film thickness less than 11~13 nm, which is close to the thickness limitation of growth in the vertical direction, the disk nanograins show a periodic array and vertical channels directly connecting the top and bottom of the film, as shown in Figure S9a. For the film thickness less than 30 nm, the nano grains on the substrate growing to 11 ~13 nm in vertical direction will stop in the thickness and continue to grow along the lateral (or radius) direction up to a radius of 22 nm (corresponding the growth limitation in radius). These well-grown nanograins form the first sub-layer followed by the vertical deposition of amorphous structure of few nanometers. Subsequently, the second sub-layer will form in the similar way, as shown in Figure S9b. The nano grains of the second sub-layer have somewhat angular distribution according to 2D GIWAXS pattern ^[3,4] and more random distribution in the horizontal direction because of the interaction with the amorphous ClAlPc molecules. For the film thickness less than 50 nm, three sub-layers could form in the similar way, as shown in Figure S9c. It is reported in the

GIWAXS and GIWAXS study on CuPc films ^[3,4] that the nano grains include the crystalline part and non-crystalline part.

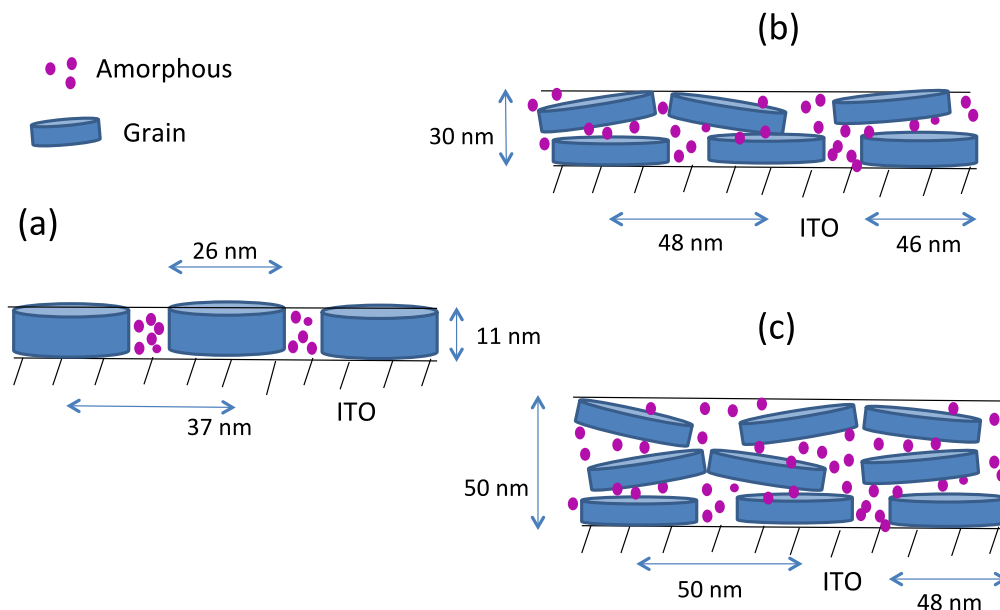


Figure S9. The proposed growth model and structure of the disk ClAlPc nano-grain in the films with thickness of (a) 10 nm, (b) 30 nm and (c) 50 nm.

For correlating the film structure with the performance or optoelectronic property, the film structure of Figure S9(a) with the direct channels in the vertical direction not only shows the best path for charge transportation but also has the least traps or defects causing recombination compared to the other film structures. The film structures of Figures S9(b) and (c) show that the amorphous region between nanograins in the vertical direction could hinder the charge transportation and provide the traps. Such amorphous regions in the vertical direction increase with increasing film thickness. The transportation path constructed by the full nanograins will play an important role in the performance improvement of solar cells and photo-detector. In contrast, the number and crystallinity of nano grains in the film could be minor factor.

Supplementary Reference

- [1] N. Kobayashi, T. Ishizaki, K. Ishii and H. Konami, *J. Am. Chem. Soc.*, 1999, **121**, 9096-9110.
- [2] P. L. Goto, M. P. Siqueira-Moura and A. C. Tedesco, *Int. J. Pharm.*, 2017, **518**, 228-241.
- [3] J. W. Kim, H. J. Kim, H. H. Lee, T. Kim and J. J. Kim, *Adv. Funct. Mater.*, 2011, **21**, 2067-2071.
- [4] H. J. Kim, J. W. Kim, H. H. Lee, T.-M. Kim, J. Jang and J.-J. Kim, *J. Phys. Chem. Lett.*, 2011, **2**, 1710-1714.
- [5] C.-Y. Chen, C.-S. Tsao, Y.-C. Huang, H.-W. Liu, W.-Y. Chiu, C.-M. Chuang, U.-S. Jeng, C.-J. Su, W.-R. Wu and W.-F. Su, *Nanoscale*, 2013, **5**, 7629-7638.
- [6] T. R. Andersen, T. T. Larsen-Olsen, B. Andreasen, A. P. Bottiger, J. E. Carle, M. Helgesen, E. Bundgaard, K. Norrman, J. W. Andreasen and M. Jørgensen, *ACS nano*, 2011, **5**, 4188-4196.
- [7] Y.-C. Huang, C.-S. Tsao, T.-Y. Huang, H.-C. Cha, D. Patra, C.-J. Su, U.-S. Jeng, K.-C. Ho, K.-H. Wei and C.-W. Chu, *J. Phys. Chem. C*, 2015, **119**, 16507-16517.
- [8] F. Liu, W. Zhao, J. R. Tumbleston, C. Wang, Y. Gu, D. Wang, A. L. Briseno, H. Ade and T. P. Russell, *Adv. Energy Mater.*, 2014, **4**, 1301377.
- [9] O. Glatter and O. Kratky, *Small angle X-ray scattering*, Academic press, 1982.
- [10] S. R. Kline, *J. Appl. Crystallogr.*, 2006, **39**, 895-900.
- [11] H.-C. Liao, C.-S. Tsao, T.-H. Lin, C.-M. Chuang, C.-Y. Chen, U.-S. Jeng, C.-H. Su, Y.-F. Chen and W.-F. Su, *J. Am. Chem. Soc.*, 2011, **133**, 13064-13073.